

Simple Dip-Coating Process for the Synthesis of Small Diameter Single-Walled Carbon Nanotubes—Effect of Catalyst Composition and Catalyst Particle Size on Chirality and Diameter

Hamid R. Barzegar,[†] Florian Nitze,[†] Tiva Sharifi,[†] Madeleine Ramstedt,[‡] Cheuk W. Tai,[§] Artur Malolepszy,^{||} Leszek Stobinski,[#] and Thomas Wågberg^{*,†}

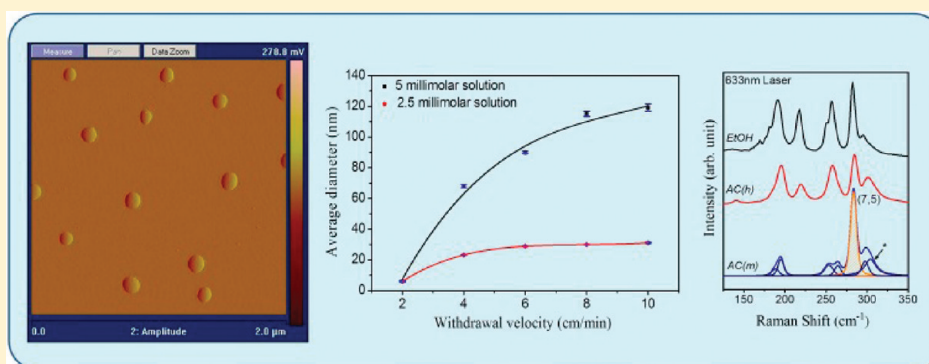
[†]Department of Physics and [‡]Department of Chemistry, Umeå University, S-901 87 Umeå, Sweden

[§]Department of Materials and Environmental Chemistry and Berzelii Center EXSELENT on Porous Materials, Arrhenius Laboratory, Stockholm University, S-106 91, Stockholm, Sweden

^{||}Faculty of Materials Science and Engineering, Warsaw University of Technology, 02-507 Warsaw, Poland

[#]Institute of Physical Chemistry, Polish Academy of Sciences Kasprzaka 48/52, 01-224 Warsaw, Poland

S Supporting Information



ABSTRACT: We report on a dip-coating method to prepare catalyst particles (mixture of iron and cobalt) with a controlled diameter distribution on silicon wafer substrates by changing the solution's concentration and withdrawal velocity. The size and distribution of the prepared catalyst particles were analyzed by atomic force microscopy. Carbon nanotubes were grown by chemical vapor deposition on the substrates with the prepared catalyst particles. By decreasing the catalyst particle size to below 10 nm, the growth of carbon nanotubes can be tuned from few-walled carbon nanotubes, with homogeneous diameter, to highly pure single-walled carbon nanotubes. Analysis of the Raman radial breathing modes, using three different Raman excitation wavelengths (488, 633, and 785 nm), showed a relatively broad diameter distribution (0.8–1.4 nm) of single-walled carbon nanotubes with different chiralities. However, by changing the composition of the catalyst particles while maintaining the growth parameters, the chiralities of single-walled carbon nanotubes were reduced to mainly four different types, (12, 1), (12, 0), (8, 5), and (7, 5), accounting for about 70% of all nanotubes.

1. INTRODUCTION

The unique properties of carbon nanotubes (CNTs) and the possibility to implement them in various applications have made them attractive for researchers in the last two decades. Despite the huge number of studies on CNTs, there are still unsolved issues regarding their exact growth mechanism.¹ In recent years, some progress has been made to selectively postpurify single-walled carbon nanotubes (SWNTs) in order to select for tubes with certain chirality, diameter, or semiconducting or metallic properties.^{2–8} However, when it comes to procedures on how to selectively grow SWNTs with predefined structures or properties, the number of successful reports is lower.^{9–13} The variations in structure and properties impose problems when SWNTs are implemented into applications, especially in photovoltaic or electronic devices.

The first reported synthesis methods for SWNTs were based on either arc discharge^{14–16} or laser ablation¹⁷ of catalyst-containing graphite. With time, however, chemical vapor deposition (CVD) has attracted more and more attention. The main reason is the capability of the method to both produce a relatively large amount of high-purity CNTs and also to gain better control of synthesis parameters.^{18,19} In addition, CVD is the only method that allows self-assembly processes and the synthesis of patterned arrays or electrodes.^{20,21} The catalytic CVD process involves the use of catalyst particles, usually as either a powder or a thin film on appropriate

Received: November 16, 2011

Revised: May 7, 2012

Published: May 8, 2012

substrates. Several studies have already shown a relationship between the catalyst particles size and the diameter of grown CNTs.^{22–25}

Dip-coating is a simple and well-known technique that has been used for several decades in industry and laboratories. This method can be used to coat different substrates with a smooth layer of a wide variety of materials.^{26,27} A liquid film will be coated on a substrate when it is vertically withdrawn from an appropriate solution. After the solvent is evaporated, depending on the experimental conditions, the substrate will be coated with a number of uniform particles or a smooth solute layer. In the past decade, this method has been applied to prepare catalyst particles for CVD growth of CNTs.^{28–30}

In this work, we present two different techniques to efficiently control the size of the catalyst nanoparticles that are deposited on a substrate. In the first method, we show that by adjusting the experimental parameters adequately in a dip-coating process, we can prepare a homogeneous distribution of nanosized catalyst particles on silicon wafers, while in the other method, we can control the size of the catalyst nanoparticles already in the solution and then transfer these to the substrate. Since the diameter of the CNTs is mainly determined by the size of the catalyst particles,³¹ the implementation of our coated substrates can be used to grow CNTs, and the diameter of the CNTs can be tailored from a narrow diameter distribution of multiwalled carbon nanotubes (MWNTs) to highly pure SWNTs. By further manipulating the catalyst particles with respect to the Co/Fe alloy, the growth can be controlled so that samples are synthesized that have a composition predominantly composed of highly pure SWNTs with subnanometer diameters and few chiralities, as verified by a Raman analysis based on several different excitation wavelengths. Our results give insight into the mechanisms of selective growth of SWNTs and will help to implement SWNTs in applications, especially when a high selectivity of SWNT types is important such as heterojunction photovoltaic and photodetector devices.³² In another perspective, our method provides appropriate starting samples for postsynthesis separation processes where a narrow chirality distribution is desired.

2. MATERIALS AND METHODS

2.1. Catalyst Precursor Preparation. In a typical experiment, iron(III) nitrate, $\text{Fe}(\text{NO}_3)_3 \cdot 9\text{H}_2\text{O}$, and cobalt(II) nitrate, $\text{Co}(\text{NO}_3)_2 \cdot 6\text{H}_2\text{O}$, both with a purity of 99.999% from Alfa Aesar, were used as catalyst precursors, and depending on the experimental condition, acetone (HPLC grade) or ethanol (99.5% purity) was used as the solvent. In each experiment, first, two separate solutions of iron nitrate and cobalt nitrate (with the same concentration) were prepared in the desired solvent. Then, both solutions were mixed and sonicated for 45 min. In our work, we have used two different methods to prepare the catalyst precursors on the substrates, which then were used for CNTs growth.

2.1.1. Ethanol Method. In this method, ethanol (EtOH) was used as a solvent to prepare catalyst precursors with a concentration of iron and cobalt in the prepared mixtures of 12.5 mM.

2.1.2. Acetone Method. Acetone was used as solvent to dissolve catalyst precursors. As in the case of the EtOH method, the concentration of iron and cobalt in the prepared mixtures was 12.5 mM. By this method, the iron nitrate did not dissolve completely in acetone but forms fluffy iron hydroxide aggregates, while cobalt nitrate dissolved completely. After

preparation, the iron nitrate suspension was mixed and sonicated together with the cobalt nitrate acetone solution, resulting in a suspension with an average particle size of several micrometers. By adding hydrochloric acid $\text{HCl}(\text{aq})$ (37%) to the suspension, the iron hydroxide aggregates partly dissolve, and thereby, the size of the iron hydroxide particles could be controlled by the HCl concentration. To facilitate this discussion, we define $R_{\text{HCl/SP}}$ as the volume ratio of HCl to suspension. In section 3, we discuss this further and introduce three different concentrations for $R_{\text{HCl/SP}}$: low, medium, and high, which all give different growth products when applied for the catalyst preparation for the CVD process. The different concentrations, with respect to the used mixture, are defined as low, $R_{\text{HCl/SP}} < 1.5 \times 10^{-3}$; medium, $R_{\text{HCl/SP}} = 1.5 \times 10^{-3}$; and high, $R_{\text{HCl/SP}} \geq 2 \times 10^{-3}$. In the final analysis, these different conditions for the acetone method are referred to as AC(l), AC(m), and AC(h).

2.2. Dip-Coating. Dip-coating was performed as follows: a piece of silicon wafer of 8 mm \times 35 mm \times 0.5 mm dimensions was first ultrasonically cleaned in acetone and subsequently treated by an ultraviolet ozone cleaner. The cleaned substrate was submerged into the bath containing the prepared solution, and after 5 min, it was withdrawn from the bath with the desired velocity. Several different solution concentrations were tested and evaluated in the dip-coating process, and thereafter, proper parameters were chosen with respect to the desired experiment.

After coating, atomic force microscopy (AFM) was used to study the topography of the samples. The analysis of the gained images was made by a software tool [Scanning Probe Image Processor (SPIP)] to measure number, diameter, and height of particles in the image.

2.3. CNTs Growth. Before CVD, the coated substrate was annealed in air at 400 °C for 15 min to form metal oxides. In a typical CVD process, the substrate was heated in Ar to 800 °C, and thereafter, an Ar/ H_2 mixture (5% H_2 ; Varigon) was introduced to the reaction chamber for 10 min to reduce the catalyst oxide particles (pretreatment).^{30,33} The growth of CNTs was carried out by adding acetylene gas to the gas flow for an experiment specific duration. Before the sample was removed, the system was cooled in Ar to below 170 °C. Experimental parameters for the growth of MWNTs and SWNTs are described in Tables 1 and 2.

Table 1. Growth Parameters for MWNTs

	temperature (°C)	time (min)	mL/min		
			Ar	Varigon	acetylene
heating	RT–800	ap. 30	180	0	0
pretreatment	800	10	125	50	0
growth	800	25	125	50	3.8
cooling	800–170		180	0	0

2.4. Sample Characterization. A multimode AFM model MMAPMLN (with Nanoscope IV controller; Veeco Metrology) and a X-ray photoelectron spectrometer (XPS, Kratos Axis Ultra DLD electron spectrometer, monochromated Al $K\alpha$ source operated at 150 W) were used to analyze the coated substrates. The CNTs were characterized by Raman spectroscopy, transmission electron microscopy (TEM), and scanning electron microscopy (SEM). TEM measurements were performed using a JEOL 2100F (200 keV) and a JEOL 1230

Table 2. Growth Parameters for SWNTs

	temperature (°C)	time (min)	mL/min		
			Ar	Varigon	acetylene
heating	RT–800	ap. 30	200	0	0
pretreatment	800	10	140	60	0
growth	800	15	140	60	3.8
cooling	800–170		200	0	0

(80 keV) on thin and holey/thin carbon film grids. SEM measurements were conducted directly on the produced sample using a Hitachi S-5500 In-lens high-resolution FE-SEM. To get information on the particle size in the acetone suspension, dynamic light scattering (DLS) using a Malvern Zetasizer nano series-ZS was employed. Commercial SWNTs (Sigma-Aldrich, Lot #MKBD4116 V Southwestern nanotechnology, diameters 0.7–0.9 nm) were used as reference sample.

2.4.1. Raman Analysis. Raman spectra were recorded using an inVia Raman Microscope (Renishaw). High wavenumber region spectra were recorded using 633 nm excitation wavelength, and in case of comparison, all spectra were normalized with respect to the G band intensity. Radial breathing modes (RBM), using three different excitation wavelengths (488, 633, and 785 nm), were recorded on 50 different spots per sample, and the average over the spectra was used for analysis. The integrated areas under the RBM peaks, used for quantitative analysis of different chiralities, were derived by employing PeakFit (v4.12) software.

3. RESULT AND DISCUSSION

In our study, we have implemented two different methods to control the size and the composition of the catalyst nanoparticles that are deposited on the CVD substrates. (i) In the first, the EtOH method (using ethanol as solvent for the metal nitrate salts), a perfect solution is obtained due to the high solubility of both iron nitrate and cobalt nitrate in ethanol. This solution is ideal for dip-coating experiments, and we show below that by varying the dip-coating parameters, such as withdrawal speed and concentrations, we can efficiently control the size of the catalyst particles that are deposited on the substrate. (ii) In the second, the acetone method (AC), the solubility of cobalt nitrate is also very high. However, the iron nitrate has lower solubility and instead forms fluffy aggregates at the bottom of the container. Investigations of these precipitates by infrared spectroscopy reveal that they consist of iron hydroxide. By adding HCl, the solubility of iron hydroxide in acetone increases (at large amounts of HCl, it again forms a perfect solution). Thus, by sonicating this suspension together with the perfect solution of cobalt nitrate, both the size and the composition of the deposited catalyst particles can be controlled. Also, with this method, dip-coating was used to deposit the catalyst nanoparticles on the substrate, but it is clear that in this case the size of the particles is less affected by the dip-coating parameters and more influenced by the predefined size of the iron hydroxide particles in the suspension (which is determined from the amount of added HCl).

We present our study by first discussing the EtOH method since this clearly shows how to tune the CNT structures from

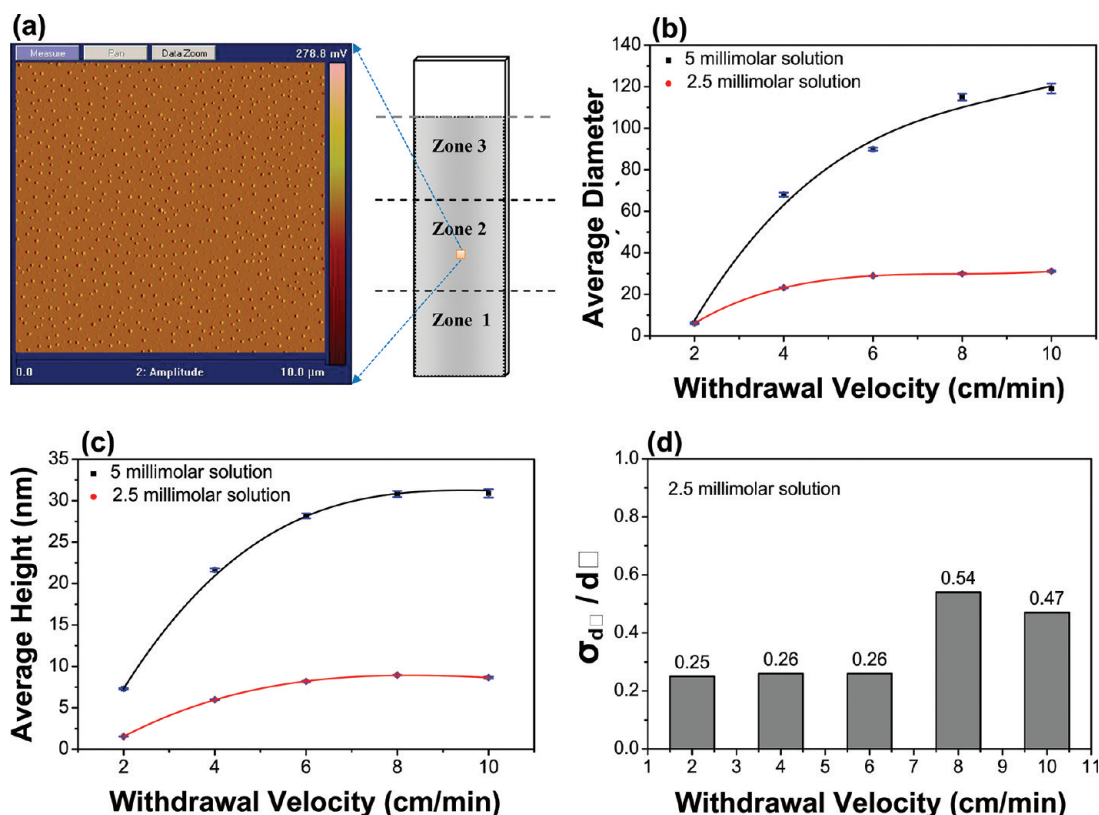


Figure 1. (a) Typical AFM image of a substrate (zone 2) dip-coated by a mixture of iron and cobalt and an illustration of the coated substrate. The dimension of the coated region (shaded region) is 8 mm \times 30 mm, which is divided into three equal zones. (b) Average particle diameter vs withdrawal velocity. (c) Average particle height vs withdrawal velocity. (d) Standard deviation of average particle diameter in zone 2 vs withdrawal velocity.

MWNTs to small diameter SWNTs, and then, we proceed by showing how the catalyst composition can be controlled in the acetone method and thereby offer the possibility to further tune the SWNTs to a narrow diameter distribution of SWNTs with few chiralities.

Figure 1a is a typical AFM image of a substrate dip-coated by an ethanol solution containing iron and cobalt. X-ray photoelectron spectroscopy (XPS) analysis (see Figure 6) and AFM images indicated that an alloy of cobalt and iron was deposited on the substrate in the form of nanoparticles after dip-coating.

For further analysis, the coated substrate was divided into three equal zones, as schematically shown in Figure 1a. The size of the catalyst particles (diameter and height), as well as the overall nanoparticle density, in different parts of the substrate were measured by AFM, and the average for all measurements was used for analysis. It should be noted that the dip-coating method suffers from edge effects; hence, the size distribution of the particles is less homogeneous on the sides of the substrate. The area of the inhomogeneous regions depends on the withdrawal velocity and is enlarged as the withdrawal velocity is increased in accordance with earlier reports.³⁴ For example, when a sample is dip-coated by 4 cm/min withdrawal, the inhomogeneous area is about 1 mm wide along the edges of the substrate. We did not consider these regions in our analysis, and no measurements were done at the edges of the samples.

Figure 1b,c shows that as the withdrawal velocity or the solutions concentration increases, the size of the catalyst particles (height and diameter) increases. To show this behavior, we have selected two specific concentrations (2.5 and 5 mM), but the same trend can be seen also for other concentrations. It can be seen that the size of the catalyst particles initially increases strongly with withdrawal velocity but then becomes less dependent, and the curve flattens out for higher velocities. Also, we observe that the size distribution of the particles in zone 2 is always more homogeneous as compared to other zones. Figure 1d shows the relative spread of the standard deviation σ_d/\bar{d} , where \bar{d} is the average particle diameter at a specific withdrawal velocity measured in zone 2 for five different withdrawal velocities. For withdrawal velocities lower than 7 cm/min, the diameter distribution is rather homogeneous, but at higher velocities, there is a significant increase in the spread of the diameters. In line with the observations, above we note that the nanoparticle density on the substrate is affected by the withdrawal velocity. This is manifested by the fact that the coverage area increases from 6.57 to 10.83% as the withdrawal velocity increased from 2 to 10 cm/min.

For each specific solution there exists a maximum withdrawal velocity over which the dimension of the catalyst particles does not increase any more (see Figure 1b,c), which is in agreement with previous studies.^{35–37} Therefore, to increase the particle size, it is necessary to increase the concentration of the solution instead of increasing the withdrawal velocity. The dip-coating process can easily be affected by the surrounding environment like temperature, air flow around the substrate, and impurity variations on the substrates. Nevertheless, tests of the reproducibility of our method show that the variation in the average particle size is only 10–20% when comparing two different samples produced with identical conditions.

3.1. CNT Growth. **3.1.1. MWCNT Growth.** Substrates with catalyst nanoparticles deposited by the EtOH method (from zone 2) were then applied in several CVD experiments to

investigate the effect of catalyst particles size on the growth of CNTs. In the large catalyst particle region where the average size of the particles is 10 nm or larger, the growth always leads to MWNTs with a narrow diameter distribution. Figure 2a is a

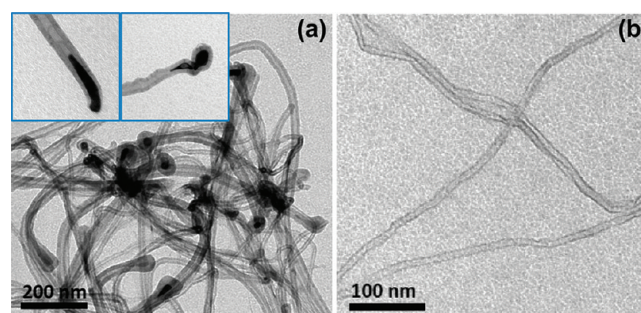


Figure 2. (a) TEM image of grown MWNTs. Insets show stretched catalyst particles at the ends of grown MWNTs. (b) Shows MWNTs with few walls.

TEM image of CNTs grown on a dip-coated substrate with catalyst particles having an average diameter of 40 ± 5 nm. This results in a growth of MWNTs with a narrow diameter distribution around 21 ± 7 nm. By decreasing the size of the catalyst particles, the growth of few-walled CNTs with small diameter was observed (Figure 2b). In all experiments resulting in growth of MWNTs, we observe a consistent correlation between the size of the catalyst particles and the diameter of the MWNTs so that the diameter of the MWNTs is approximately 45–50% smaller than the average diameter of the catalyst particles. This agrees well with the in situ study by Lin et al.³¹ and is rationalized by a growth model where the catalyst particles are stretched by diffusing carbon atoms during the growth process. Insets in Figure 2a show the stretched catalyst particles that are encapsulated inside and at the tips of the tubes. A further explanation for the difference between the diameter of the MWNTs and the catalyst particles can be that the catalyst particles still contain small amounts of solvents when characterized by the AFM. The remaining solvent is then evaporated during the calcination of the substrate.

3.1.2. SWCNT Growth. A further decrease in catalyst particle size below 10 nm led to the growth of SWNTs, also in good agreement with previous studies.³¹ It should be noted that it is important to vary the amount of carbon precursor introduced into the reaction chamber according to the size of the catalyst particle used; the smaller the catalyst particles, the lower the amount of carbon precursor. This is manifested by the fact that the synthesis on catalyst particles smaller than 50 nm in combination with a high amount of acetylene yielded no CNT growth. This observation is in agreement with Yoon et al.³⁸ who explained that the deactivation by an excess carbon concentration in small catalyst particles was created by a too high amount of acetylene. To avoid this effect, the acetylene gas was diluted by an increasing flow of the carrier gases with decreasing catalyst particle size (please see Tables 1 and 2). Figure 3a displays a Raman spectrum obtained by a He–Ne laser (633 nm) of as-grown SWNTs in the small catalyst particle regime (<10 nm), using the EtOH method to prepare catalyst-decorated substrate.

The growth of SWNTs was confirmed by the presence of a sharp and strong G band and distinct RBMs in the Raman spectra.³⁹ The D band, centered at 1310 cm^{-1} , is related to the presence of impurities, amorphous carbon, and structural

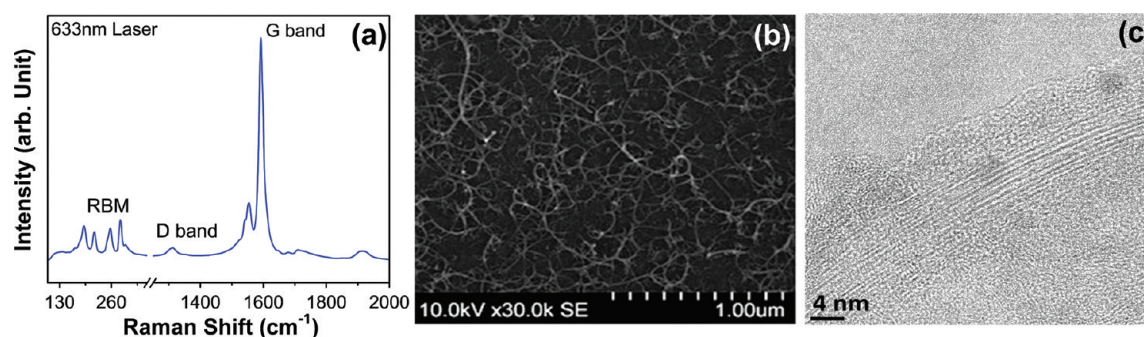


Figure 3. (a) Typical Raman spectra, (b) SEM, and (c) TEM images of as-grown SWNTs on a substrate that was dip-coated by a mixture of iron and cobalt using ethanol as a solvent.

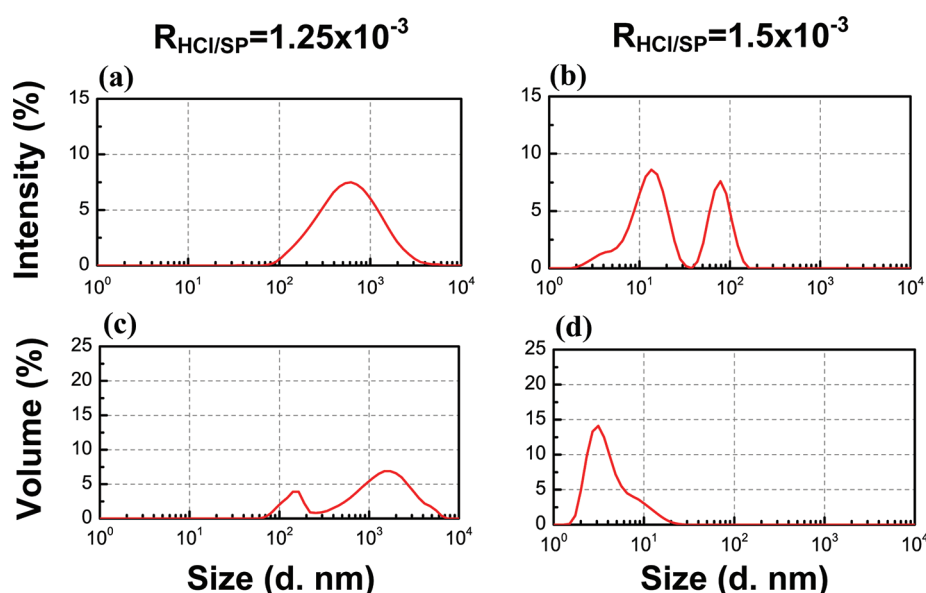


Figure 4. Evaluation of particle size in the suspension [prepared by mixing iron(III) nitrate and cobalt(II) nitrate in acetone] using DLS for two different values of $R_{\text{HCl/SP}}$ (a) low region 1.25×10^{-3} and (b) medium value 1.5×10^{-3} . Panels a and b show the intensity distribution of the scattered light vs particles size, while panels c and d show the total volume of particles as a function of their size.

defects in SWNTs,⁴⁰ and the integrated intensity ratio of the G to D band ($I_{\text{G}}/I_{\text{D}}$) is frequently used to estimate the degree of crystallinity of SWNTs.^{41,42} The $I_{\text{G}}/I_{\text{D}}$ of our as-grown SWNTs was 18.2 significantly higher than a highly purified commercial SWNTs reference sample with a similar diameter distribution [$I_{\text{G}}/I_{\text{D}}$ of 9; see Figure S(3) in the Supporting Information]. This signals a growth of highly crystalline SWNTs with low amounts of amorphous side products. The frequencies of the RBM peaks (ω_{RBM}) are inversely proportional to the tube diameters (d_{t}) through the relation $\omega_{\text{RBM}} = A/d_{\text{t}} + B$, where A and B are experimentally determined parameters depending on SWNT diameter, having different values for bundles of SWNT and isolated SWNT.⁴³ Because the RBMs in Figure 3 consist of several peaks in the frequency range of 170–300 cm⁻¹, we can conclude that the produced sample contains a relatively broad diameter distribution of SWNTs with many different chiralities. In an extended analysis with several different excitation wavelengths (discussed later in the text) and by using previously assigned RBM frequency values for specific tubes,^{43–45} we show that the samples produced by the process described above contain numerous chiralities in the diameter range from 0.8 to 1.4 nm. Figure 3b,c shows SEM and high-resolution TEM images of the SWNTs, which tend to form bundles, in agreement with earlier studies.⁴⁶

Various different conditions were tested and evaluated to grow small SWNTs with a narrow diameter distribution using the ethanol dip-coating process. However, under no condition could we fine-tune the process further to yield a more selective growth than the SWNTs described in Figure 3.

To further increase the selectivity in the growth process, we have therefore developed and evaluated the acetone method (AC), which is described in the first paragraph in section 3 and in the experimental section 2. The combination of iron(III) nitrate, which *does not dissolve* completely in acetone but rather formed a fluffy iron hydroxide precipitate at the bottom of the container, with the cobalt(II) nitrate, which *dissolves* completely, enables control of both the particle sizes deposited on the substrate and the particle compositions (ratio of Fe/Co). This is based on the fact that the particle size of the iron hydroxide particles in the acetone solution can be manipulated by adding HCl in a controlled manner. The dip-coating process enables us to “fish up” these iron hydroxide particles together with the cobalt solution, and after annealing, these form alloys of Fe/Co, which according to XPS data have slightly different ratios depending on the size of the iron hydroxide particles and concentration of cobalt in the solution. Figure 4 shows the resulting particle size derived from an analysis based on DLS at 25 °C for two different values of $R_{\text{HCl/SP}}$. Figure 4a,b shows the

intensity distributions of scattered light. Because larger particles scatter more light compared to smaller particles, these plots do not represent the true quantitative distribution for the number of particles with a specific size. To recalculate the data into volume distributions, the refractive index of the particles in the suspension was estimated to be equal to the refractive index of goethite (FeOOH). The resulting volume distributions show the volume of particles of different sizes (Figure 4c,d).

Figure 4a shows DLS data for a $R_{\text{HCl/SP}}$ ratio of 1.25×10^{-3} (low $R_{\text{HCl/SP}}$ region). At this concentration, the diameter distribution of the particles is broad and in the range of 100 nm to 6.0 μm but with the largest volume of particles around 1.0 μm (Figure 4c). By increasing $R_{\text{HCl/SP}}$ to 1.5×10^{-3} (medium value), the particle diameters decreased drastically, and the largest volume of particles has diameters between 1.5 and 5 nm (see Figure 4b,d). At this stage, the dispersion is clear and looks like a true solution. A further increase of $R_{\text{HCl/SP}}$ to 2×10^{-3} or higher (high $R_{\text{HCl/SP}}$ region) turned the mixture to a perfect solution, and the DLS measurement did not show any particles. A similar trend was observed for different concentrations of metal species in the suspension. The observations above are rationalized by the high solubility of iron hydroxide in HCl and by adding HCl to the suspension iron hydroxide particles partially dissolved, resulting in a decreased particle size. When $R_{\text{HCl/SP}}$ is high enough, all iron hydroxide dissolves, and the suspension becomes a perfect solution. The sizes of the particles estimated by the DLS measurements are further confirmed by AFM measurements on the dip-coated substrates [see the Supporting Information, Figures S1(a) and S1(b)].

Thus, CVD process on the catalyst-decorated substrate, using the acetone method with low values of $R_{\text{HCl/SP}}$ (when the diameters of the particles within the suspension are larger than 10 nm), always gives rise to growth of MWNTs with a broad diameter distribution. At high values of $R_{\text{HCl/SP}}$ (when all of the iron hydroxide particles were dissolved), the CVD process on the dip-coated substrates resulted in the growth of only SWNTs with a diameter and chirality distribution similar to the one obtained by the EtOH method. This is clear by comparing spectra AC(h) and EtOH in Figure 5a–d, which show the Raman spectra of a typical sample produced by the acetone method at high $R_{\text{HCl/SP}}$ together with the spectrum of a sample produced by the EtOH method, respectively.

However, using medium values of $R_{\text{HCl/SP}} = 1.5 \times 10^{-3}$ with a suspension consisting mainly of particles less than 5 nm [see Figure 4d and Figure S1(b) in the Supporting Information] led to the growth of predominantly SWNTs with a small fraction of MWNTs (as indicated by TEM images). Spectrum AC(m) in Figure 5a shows the high-frequency Raman spectrum of a typical sample produced by the acetone method at medium value of $R_{\text{HCl/SP}}$, obtained by a 633 nm laser. The $I_{\text{G}}/I_{\text{D}}$ ratio decreases in the spectrum AC(m) as compared to spectra EtOH and AC(h) (all of the three spectra are normalized with respect to G band), related to the presence of few MWNTs.⁴⁷

More importantly is however that all SWNTs grown under these conditions (acetone method, medium $R_{\text{HCl/SP}}$) exhibited a very narrow diameter range with only few chiralities. This is clear from spectra AC(m) in Figure 5b–d, indicating the RBM region of such samples. The RBMs can be used to evaluate the amount of different types of SWNTs in the sample.^{13,48,49} Analyzing and comparing the RBMs, by all three excitation lasers, reveals that the ratio of the (7,5), (8,5), (12,1), and (12,0) tubes to all of the observed chiralities in the sample significantly increases from 29.9% in the spectra AC(h) to

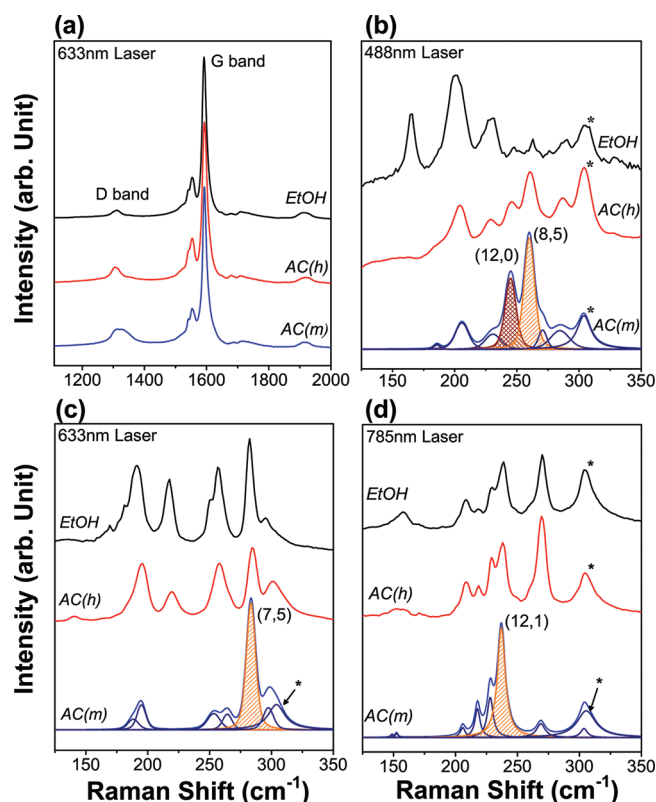


Figure 5. Raman spectra of as-grown SWCNTs. (a) Comparison of high-frequency spectra of samples produced by the ethanol method, acetone method at high $R_{\text{HCl/SP}}$ [AC(m)] and acetone method at medium $R_{\text{HCl/SP}}$. (b–d) RBM of the same samples obtained by using three different excitation wavelengths: 488, 633, and 785 nm. Each spectrum in the RBM frequency range is an average of over 50 measurements on different randomly selected spots of the sample. The * in panels b–d indicates the Si peak at about 303 cm^{-1} , originating from the substrate.

68.4% in the spectra AC(m). The predominated tubes are represented by RBMs at 283, 260, 238, and 246 cm^{-1} , respectively.^{44,45} We note that neither the (12, 0) nor the (8, 5) tube are in full resonance with the 488 nm probing laser, but yet still clearly are detectable in agreement with earlier reports.⁴⁵ We hypothesize that the increase in yield of the specific types of SWNTs by the acetone method, using medium $R_{\text{HCl/SP}}$, is initiated by the presence of iron hydroxide particles with certain size in the suspension. According to Ding et al.⁵⁰ and other studies,^{51–53} the growth of SWNTs highly depends on the adhesion strength between metal catalyst particles and the carbon atoms of the extruding SWNTs. Too high or too low adhesion strength leads to either no growth or growth of non-SWNT products. Also, since the adhesion energy depends on the chirality of the SWNTs, it is plausible that a suitable catalyst particle composition can lead to growth of certain stable chiralities “fitting” the adhesion strength window of the actual metal alloy. To evaluate this model, we have performed XPS measurements on the catalyst-coated substrates.

Figure 6 shows the wide XPS spectra of the dip-coated substrates by using the three different methods. The N 1s peak observed in all spectra is related to NO_3^- originating from the catalyst precursors. In addition, Cl 2s and Cl 2p peaks are observed only in spectra AC(h) and AC(m), which originated from HCl added to the suspension during catalyst precursor preparation. By measuring the Fe/Co ratio from the high-

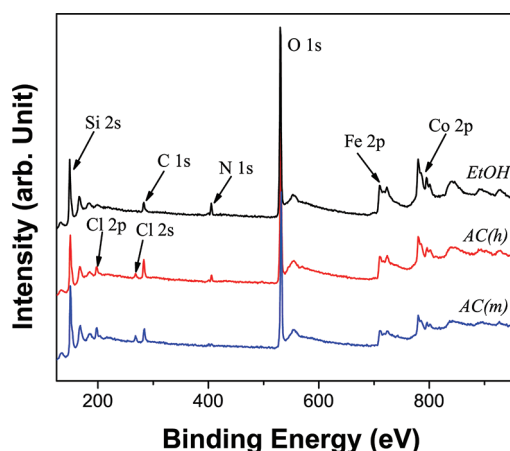


Figure 6. XPS wide spectra of dip-coated substrates using EtOH method, acetone method at high $R_{\text{HCl/SP}}$ values [AC(h)], and acetone method at medium value of $R_{\text{HCl/SP}}$ [AC(m)]. Peaks are assigned in the figure.

resolution XPS data, we observe that by using the EtOH method, the Fe/Co ratio of the catalyst particles on the substrate is very close to 1 (0.99 ± 0.04). By using the acetone method with the medium $R_{\text{HCl/SP}}$ value, the Fe/Co ratio changes to 1.12 ± 0.03 , while using high values of $R_{\text{HCl/SP}}$ again bring the Fe/Co ratio back close to 1 (1.06 ± 0.01). Although the differences in the measured Fe/Co ratios are small, it still supports the idea that the reproducible selective growth originates from differences in catalyst particle composition. This argumentation stems from the fact that the CVD experiments performed at these three different conditions all are based on catalyst particles with similar size [below 5 nm, please see Figures 3d and S1(a) in the Supporting Information]; yet, only one set of conditions gives rise to the selective growth of few chiralities. We rationalize that the difference in Fe/Co ratio originates from the iron hydroxide particles in the suspension and has sizes that depend on $R_{\text{HCl/SP}}$ values. This results in the formation of catalyst particles where different ratios of cobalt can diffuse into the iron hydroxide particles. At certain Fe/Co ratios, this might lead to a stronger adhesion between metal particles and diffusing carbon atoms. In combination with the regular requirements of catalyst particle size, this leads to a preferred growth of the most energetically stable tubes, namely, the (7, 5), (8, 5), (12, 0), and the (12, 1). All of these tubes are either near armchair [(7, 5) and (8, 5)], zigzag (12, 0), or near zigzag (12, 1) and have been reported to possess a certain high stability among SWNTs with diameters below 1 nm.¹¹ The high relative abundance of the (12, 1) chirality observed in our study, in contrast to other reports,^{10,11} is likely caused by the fact that those studies utilized photoluminescence to investigate the samples, but this characterization technique is well-known to underestimate the presence of SWNTs with low chiral angles (i.e., zigzag).¹⁰ We note however, also that in a recent study it has been manifested that SWNTs with large chiral angles are expected to grow longer as compared to SWNTs with small chiral angles. This is worth noticing since it could lead to an overestimation of such tubes by, for example, Raman studies. In our study, we, however, do not believe that such an effect is present, since we see very small contributions of the (n, n) tubes ($\theta = 30^\circ$) and a large contribution of the achiral (12, 0) tubes ($\theta = 0^\circ$). Our study supports theoretical calculations showing that the control

of size and composition of catalyst nanoparticles are very important aspects in how to achieve selective growth of SWNTs and that this process can be a good alternative to the previously used methods to control the synthesis parameters.⁴¹

4. CONCLUSIONS

We have shown that by tuning the experimental conditions in a dip-coating process, we can precisely control the size of the metal catalyst particles deposited on a substrate. This allows us to grow MWNTs and SWNTs with a narrow range of diameters. At the optimized conditions, by changing the catalyst composition (ratio of Fe/Co), our method leads to the growth of SWNTs that are strongly dominated (70%) by four types of tubes, the (7, 5), (8, 5), (12, 0), and (12, 1) tubes. Our study gives further insight into how monodisperse samples of SWNTs can be grown selectively.

■ ASSOCIATED CONTENT

Supporting Information

AFM images, comparison of Raman spectra of as-grown SWNTs, and reference sample. This material is available free of charge via the Internet at <http://pubs.acs.org>.

■ AUTHOR INFORMATION

Corresponding Author

*E-mail: Thomas.wagberg@physics.umu.se.

Notes

The authors declare no competing financial interest.

■ ACKNOWLEDGMENTS

This work was supported by grants from the Swedish research council (dnr: 2010-3973). T.W. and H.R.B. acknowledge the vibrational spectroscopy platform (ViSP) at Umeå University. T.W. thanks Magnus Bergvalls stiftelse and Ångpanneföreningen for support. F.N. thanks Kempestiftelsen and Gustaf Richerts stiftelse for support. A.M. thanks the European Union in the framework of European Social Fund through the Warsaw University of Technology Development Programme and L.S. thanks Polish Council for Science for grant (KB/72/13447/IT1-B/U/08). The Knut and Alice Wallenberg Foundations are acknowledged for an equipment grant for the electron microscopy facilities in Stockholm University. Dr. Andrey Shchukarev at Umeå University is acknowledged for performing the XPS measurements.

■ REFERENCES

- (1) Zhao, N. Q.; He, C. N.; Jiang, Z. Y.; Li, J. J.; Li, Y. D. *Mater. Lett.* **2006**, *60*, 159–163.
- (2) Hersam, M. C. *Nature Nanotechnol.* **2008**, *3*, 387–394.
- (3) Strano, M. S.; Dyke, C. A.; Usrey, M. L.; Barone, P. W.; Allen, M. J.; Shan, H. W.; Kittrell, C.; Hauge, R. H.; Tour, J. M.; Smalley, R. E. *Science* **2003**, *301*, 1519–1522.
- (4) Rinzler, A. G. *Nature Nanotechnol.* **2006**, *1*, 17–18.
- (5) Kim, W. J.; Usrey, M. L.; Strano, M. S. *Chem. Mater.* **2007**, *19*, 1571–1576.
- (6) Chattopadhyay, D.; Galeska, L.; Papadimitrakopoulos, F. *J. Am. Chem. Soc.* **2003**, *125*, 3370–3375.
- (7) Kim, S. N.; Luo, Z. T.; Papadimitrakopoulos, F. *Nano Lett.* **2005**, *5*, 2500–2504.
- (8) Balasubramanian, K.; Sordan, R.; Burghard, M.; Kern, K. *Nano Lett.* **2004**, *4*, 827–830.
- (9) Ding, L.; Tselev, A.; Wang, J. Y.; Yuan, D. N.; Chu, H. B.; McNicholas, T. P.; Li, Y.; Liu, J. *Nano Lett.* **2009**, *9*, 800–805.

- (10) Wang, B.; Poa, C. H. P.; Wei, L.; Li, L. J.; Yang, Y. H.; Chen, Y. *J. Am. Chem. Soc.* **2007**, *129*, 9014–9019.
- (11) Bachilo, S. M.; Balzano, L.; Herrera, J. E.; Pompeo, F.; Resasco, D. E.; Weisman, R. B. *J. Am. Chem. Soc.* **2003**, *125*, 11186–11187.
- (12) Harutyunyan, A. R.; Chen, G. G.; Paronyan, T. M.; Pigos, E. M.; Kuznetsov, O. A.; Hewaparakrama, K.; Kim, S. M.; Zakharov, D.; Stach, E. A.; Sumanasekera, G. U. *Science* **2009**, *326*, 116–120.
- (13) Qu, L. T.; Du, F.; Dai, L. M. *Nano Lett.* **2008**, *8*, 2682–2687.
- (14) Iijima, S. *Nature* **1991**, *354*, 56–58.
- (15) Journet, C.; Maser, W. K.; Bernier, P.; Loiseau, A.; delaChapelle, M. L.; Lefrant, S.; Deniard, P.; Lee, R.; Fischer, J. E. *Nature* **1997**, *388*, 756–758.
- (16) Liu, B. B.; Wågberg, T.; Olsson, E.; Yang, R. S.; Li, H. D.; Zhang, S. L.; Yang, H. B.; Zou, G. T.; Sundqvist, B. *Chem. Phys. Lett.* **2000**, *320*, 365–372.
- (17) Rinzler, A. G.; Liu, J.; Dai, H.; Nikolaev, P.; Huffman, C. B.; Rodriguez-Macias, F. J.; Boul, P. J.; Lu, A. H.; Heymann, D.; Colbert, D. T.; et al. *Appl. Phys. A: Mater. Sci. Process.* **1998**, *67*, 29–37.
- (18) Thostenson, E. T.; Ren, Z. F.; Chou, T. W. *Compos. Sci. Technol.* **2001**, *61*, 1899–1912.
- (19) Chen, T. T.; Liu, Y. M.; Sung, Y.; Wang, H. T.; Ger, M. D. *Mater. Chem. Phys.* **2006**, *97*, 511–516.
- (20) Downard, A. J.; Liu, X.; Baronian, K. H. R. *Anal. Chem.* **2008**, *80*, 8835–8839.
- (21) Hsiou, Y. F.; Yang, Y. J.; Stobinski, L.; Kuo, W.; Chen, C. D. *Appl. Phys. Lett.* **2004**, *84*, 984–986.
- (22) Choi, Y. C.; Shin, Y. M.; Lim, S. C.; Bae, D. J.; Lee, Y. H.; Lee, B. S.; Chung, D. C. *J. Appl. Phys.* **2000**, *88*, 4898–4903.
- (23) Wei, Y. Y.; Eres, G.; Merkulov, V. I.; Lowndes, D. H. *Appl. Phys. Lett.* **2001**, *78*, 1394–1396.
- (24) Chhowalla, M.; Teo, K. B. K.; Ducati, C.; Rupasinghe, N. L.; Amaratunga, G. A. J.; Ferrari, A. C.; Roy, D.; Robertson, J.; Milne, W. I. *J. Appl. Phys.* **2001**, *90*, 5308–5317.
- (25) Ho, G. W.; Wee, A. T. S.; Lin, J.; Tjiu, W. C. *Thin Solid Films* **2001**, *388*, 73–77.
- (26) Baigl, D.; Le Berre, M.; Chen, Y. *Langmuir* **2009**, *25*, 2554–2557.
- (27) Rizzato, A. P.; Santilli, C. V.; Pulcinelli, S. H. *J. Sol-Gel Sci. Technol.* **2000**, *19*, 811–816.
- (28) Ortiz-Lopez, J.; Ortega-Cervantez, G.; Rueda-Morales, G. J. *Mater. Sci.: Mater. Electron.* **2009**, *20*, 403–407.
- (29) Ortega-Cervantez, G.; Rueda-Morales, G.; Ortiz-Lopez, J. *Microelectron. J.* **2005**, *36*, 495–498.
- (30) Maruyama, S.; Einarsson, E.; Murakami, Y.; Edamura, T. *Chem. Phys. Lett.* **2005**, *403*, 320–323.
- (31) Lin, M.; Tan, J. P. Y.; Boothroyd, C.; Loh, K. P.; Tok, E. S.; Foo, Y. L. *Nano Lett.* **2006**, *6*, 449–452.
- (32) Bindl, D. J.; Wu, M. Y.; Prehn, F. C.; Arnold, M. S. *Nano Lett.* **2011**, *11*, 455–460.
- (33) Nitze, F.; Andersson, B. M.; Wågberg, T. *Phys. Status Solidi B* **2009**, *246*, 2440–2443.
- (34) Arfsten, N. J.; Eberle, A.; Otto, J.; Reich, A. J. *Sol-Gel Sci. Technol.* **1997**, *8*, 1099–1104.
- (35) Krozel, J. W.; Palazoglu, A. N.; Powell, R. L. *Chem. Eng. Sci.* **2000**, *55*, 3639–3650.
- (36) Groenvel, P. J. *Paint Technol.* **1971**, *43*, 50.
- (37) Gledhill, S.; Koehler, T.; Grimm, A.; Allsop, N.; Camus, C.; Hansel, A.; Bohne, W.; Rohrich, J.; Lux-Steiner, M.; Fischer, C. H. *Thin Solid Films* **2009**, *517*, 3332–3339.
- (38) Yoon, Y. J.; Bae, J. C.; Baik, H. K.; Cho, S.; Lee, S. J.; Song, K. M.; Myung, N. S. *Chem. Phys. Lett.* **2002**, *366*, 109–114.
- (39) Rao, A. M.; Richter, E.; Bandow, S.; Chase, B.; Eklund, P. C.; Williams, K. A.; Fang, S.; Subbaswamy, K. R.; Menon, M.; Thess, A.; et al. *Science* **1997**, *275*, 187–191.
- (40) Herrera, J. E.; Balzano, L.; Pompeo, F.; Resasco, D. E. *J. Nanosci. Nanotechnol.* **2003**, *3*, 133–138.
- (41) Picher, M.; Anglaret, E.; Arenal, R.; Jourdain, V. *ACS Nano* **2011**, *5*, 2118–2125.
- (42) Kwok, C. T. M.; Reizman, B. J.; Agnew, D. E.; Sandhu, G. S.; Weistroffer, J.; Strano, M. S.; Seebauer, E. G. *Carbon* **2010**, *48*, 1279–1288.
- (43) Dresselhaus, M. S.; Dresselhaus, G.; Saito, R.; Jorio, A. *Phys. Rep.—Rev. Sect. Phys. Lett.* **2005**, *409*, 47–99.
- (44) Bachilo, S. M.; Strano, M. S.; Kittrell, C.; Hauge, R. H.; Smalley, R. E.; Weisman, R. B. *Science* **2002**, *298*, 2361–2366.
- (45) Strano, M. S.; Doorn, S. K.; Haroz, E. H.; Kittrell, C.; Hauge, R. H.; Smalley, R. E. *Nano Lett.* **2003**, *3*, 1091–1096.
- (46) Thess, A.; Lee, R.; Nikolaev, P.; Dai, H. J.; Petit, P.; Robert, J.; Xu, C. H.; Lee, Y. H.; Kim, S. G.; Rinzler, A. G.; et al. *Science* **1996**, *273*, 483–487.
- (47) Eres, G.; Kinkhabwala, A. A.; Cui, H. T.; Geohegan, D. B.; Puretzky, A. A.; Lowndes, D. H. *J. Phys. Chem. B* **2005**, *109*, 16684–16694.
- (48) Krupke, R.; Hennrich, F.; von Lohneysen, H.; Kappes, M. M. *Science* **2003**, *301*, 344–347.
- (49) Huang, H. J.; Maruyama, R.; Noda, K.; Kajiura, H.; Kadono, K. *J. Phys. Chem. B* **2006**, *110*, 7316–7320.
- (50) Ding, F.; Larsson, P.; Larsson, J. A.; Ahuja, R.; Duan, H. M.; Rosen, A.; Bolton, K. *Nano Lett.* **2008**, *8*, 463–468.
- (51) Reich, S.; Li, L.; Robertson, J. *Phys. Rev. B* **2005**, *72*, 8.
- (52) Lolli, G.; Zhang, L. A.; Balzano, L.; Sakulchaicharoen, N.; Tan, Y. Q.; Resasco, D. E. *J. Phys. Chem. B* **2006**, *110*, 2108–2115.
- (53) Rodriguez-Manzo, J. A.; Terrones, M.; Terrones, H.; Kroto, H. W.; Sun, L. T.; Banhart, F. *Nature Nanotechnol.* **2007**, *2*, 307–311.
- (54) Ding, F.; Harutyunyan, A. R.; Yakobson, B. I. *Proc. Natl. Acad. Sci. U.S.A.* **2009**, *106*, 2506–2509.